AFRL-AFOSR-VA-TR-2019-0285

Chiral-Selective Carbon Nanotube Growth New, Clear horizons from Theory to Practice

Boris Yakobson
WILLIAM MARSH RICE UNIV HOUSTON TX

09/17/2019
Final Report

Air Force Research Laboratory
AF Office Of Scientific Research (AFOSR)/ RTB2
Arlington, Virginia 22203
Air Force Materiel Command

REPORT DOCUMENTATION PAGE

Form Approved
OMB No. 0704-0188

1. REPORT DATE *(DD-MM-YYYY)*	**2. REPORT TYPE**	**3. DATES COVERED** *(From - To)*
09/12/2019	Final report	05/31/2014 to 06/01/2018

4. TITLE AND SUBTITLE
Chiral-Selective Carbon Nanotube Growth New, Clear horizons

5a. CONTRACT NUMBER
FA9550-14-1-0107

5b. GRANT NUMBER
FA9550-14-1-0107

5c. PROGRAM ELEMENT NUMBER

6. AUTHOR(S)
Boris. I. Yakobson

5d. PROJECT NUMBER

5e. TASK NUMBER

5f. WORK UNIT NUMBER

7. PERFORMING ORGANIZATION NAME(S) AND ADDRESS(ES)
Rice University
6100 Main Street, MS 325
Houston, TX 77005

8. PERFORMING ORGANIZATION REPORT NUMBER

9. SPONSORING/MONITORING AGENCY NAME(S) AND ADDRESS(ES)
AFOSR
875 North Randolph Street
Arlington, VA 22203

10. SPONSOR/MONITOR'S ACRONYM(S)

11. SPONSOR/MONITOR'S REPORT NUMBER(S)

12. DISTRIBUTION/AVAILABILITY STATEMENT
Distribution A - Approved for public release

13. SUPPLEMENTARY NOTES

14. ABSTRACT

The growth of nanotubes with specific chirality is essential for industrial applications and remains a great challenge. Using graphene as a for the representation of the CNT edge, we investigated effects of catalyst type and softness on preferred positioning of the edge as well as its growth shapes. Considering the energetics of the CNT-catalyst interface, we uncovered an edge-type segregated configuration that significantly lowers the energy of chiral nanotubes allowing preference towards mid-chirality CNTs on some catalysts, while combination of the thermodynamic preference towards armchair CNTs on Co and Ni catalysts and kinetic favoring of chiral tubes explained the next-to-armchair chiral preference. Those findings provide rich theoretical base for the CNT synthesis with controlled chiral selectivity.

15. SUBJECT TERMS
carbon, nanotubes, chirality, selective growth, modeling

16. SECURITY CLASSIFICATION OF:			**17. LIMITATION OF ABSTRACT**	**18. NUMBER OF PAGES**	**19a. NAME OF RESPONSIBLE PERSON**
a. REPORT	**b. ABSTRACT**	**c. THIS PAGE**			Boris I. Yakobson
					19b. TELEPHONE NUMBER *(Include area code)*
UU	UU	UU	UU	7	713-348-3572

Final Performance Report

Contract/Grant Title:	Chiral-selective carbon nanotube growth: New, clear horizons
Contract/Grant #:	FA9550-14-1-0107
Principal Investigator:	Boris I. Yakobson
Performing Organization:	Rice University
Full Reporting Period:	06/01/2014 – 05/31/2018

The broad interest in carbon nanotubes (CNTs), unceasing since their first clear observation, has been fueled by possible technological applications derived from their unique fundamental properties. CNT's chirality – the direction of hexagonal carbon lattice within nanotube specified by the indexes (n, m) – defines its atomistic structure as well as its properties. Hence, the creation or growth of nanotubes with predetermined chirality is essential for industrial applications and remains a great challenge, despite some experimental success in recent years (see Fig. 1). Using graphene as a simplified representation of the CNT edge, we explore preferences in its relative position compared to the substrate. We find that depending on softness of the catalyst metal either sunk (or docked to the metal step) or on-terrace position can be favored. A closer look at the epitaxial graphene-catalyst epitaxial interaction allowed an explanation of various growth shapes through symmetry breaking. We investigated the energetics of the CNT-catalyst interface as one of the factors determining the chiral preference during the nanotube nucleation and uncovered a previously overlooked edge-type segregated configuration that significantly lowers the energy of chiral nanotubes in contact with the catalyst surface allowing preference towards mid-chirality CNTs on catalyst without strong preference between armchair and zigzag tubes. At the same time combination of the thermodynamic preference towards armchair CNTs on Co and Ni catalysts and kinetic favoring of chiral tubes explained the next-to-armchair chiral preference. Those findings provide rich theoretical base for the CNT synthesis with controlled chiral selectivity.

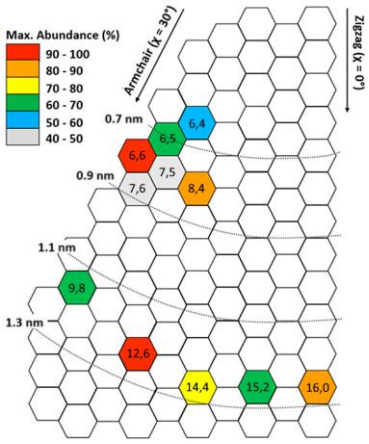

Figure 1. Recent advances toward chirality controlled SWCNT growth. Chiral index map showing the (n,m) indices of all the SWCNTs that have been grown with high purity. The maximum reported abundance for each nanotube is shown with color. [1]

Sharing the same hexagonal carbon lattice, graphene and CNT are inevitably similar in some regards. Indeed, the graphene growth process can shed some light on the growth mechanism of carbon nanotubes and, in some cases, can be used to simplify the simulation system without compromising observed tendencies. We use such setup for consideration of the CNT edge (represented by graphene edge) "wetting" by the catalyst. The main positions of the graphene on the substrate – sunk (S) and on-terrace (OT) (see Fig.2 a) – correspond to specific positions of the CNT edge on the catalyst particle. Surprisingly, the preferred modes are not the same but vary from metal to metal.

Different from that on a terrace, the matching between the graphene edge and the metal step plays a crucial role in the stability of the interface. For example, the structure of the most stable $(01\bar{1})$ step on the fcc(111) surface is characterized by all the step atoms aligned in a straight line (Fig.2b). Among all potential graphene edges, only zigzag (ZZ) and armchair (AC) ones present the same characteristics. One can

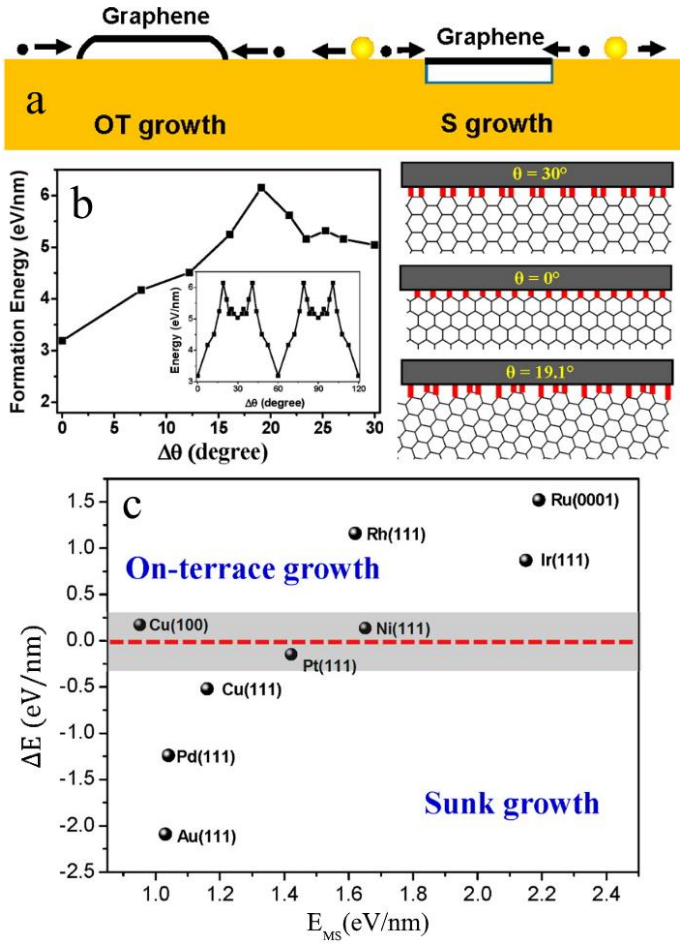

Figure 2. (a) Schematic representation of two regimes of graphene growth: on-terrace and sunk. (b) Formation energies of the interfaces between various graphene edge and $(01\bar{1})$ metal step on Cu (111) surface vs the graphene/Cu (111) misorientation angle θ and an illustration of edge binding to Cu step. (c) Relationship between formation energy of metal step (E_{MS}) and ΔE. For metals with small E_{MS} (soft metals such as Au, Pd, and Cu), the S growth mode is preferred, whereas for metals with large E_{MS} (hard metals such as Ni, Rh, Ru, and Ir) the OT growth mode dominates. [2]

imagine that an AC or ZZ type graphene edge is able to match a $(01\bar{1})$ step perfectly because all the atoms of the edge can bind with the metal step strongly (Figure 2b, θ = 0°, 30°). Once the edge deviates from AC or ZZ, it is difficult for a kinky graphene edge to match the $(01\bar{1})$ metal step and, thus, leads to some edge atoms are closer to the step than others (Figure 2c). This mismatching makes the strong binding of all edge atoms to the metal step impossible. So, we can anticipate that the AC and ZZ edges are the two types of edges that can form a more stable interface with the $(01\bar{1})$ metal step.

To explore the feasibility of S growth, we define the formation energy difference between the S and OT growth modes as

$$\Delta E = E_S(G) + E_{MS} - E_T(G),$$

where $E_T(G)$ and $E_S(G)$ are the formation energies of the graphene edge on the metal terrace and attached to a $(01\bar{1})$ metal step, respectively. E_{MS} refers to the formation energy of a $(01\bar{1})$ metal step. $E_S(G) + E_{MS}$ can be considered as the formation energy of a sunk graphene edge because it requires the creation of both a metal step and the attachment of a graphene edge on it. $\Delta E < 0$ indicates that the S growth is more favorable than the OT growth and vice visa. We found that depending on the energies of graphene-edge "wetting" by the catalyst: on a catalyst surface of soft metal like Au(111), Cu(111) or Pd(111), the graphene tends to grow in step-attached or embedded mode, while on a rigid catalyst surface such as Pt(111), Ni(111), Rh(111), Ir(111), or Ru(0001), graphene prefers growing as step-attached or on-terrace (Fig.2c). Accordingly, as further energy analysis shows, the graphene formed via the SA modes should have orientations fixed relative to the metal crystal lattice, thus prescribing epitaxial growth of graphene on Au(111), Cu(111) and Pd(111). This conclusion indeed correlates well with numerous experimental data and suggests better ways for growing single-crystalline graphene and nanotubes by making proper catalyst selections.

Interaction with the underlying substrate is crucially important for both CNT and graphene growth. In graphene growth, island symmetry can become lower than the intrinsic symmetries of both graphene and the catalyst [3]. We used the first-principles calculations and Monte Carlo modeling to explain the shapes observed in experiments and earlier studies for various metal surface symmetries. For equilibrium shape, edge energy variations δE manifest in distorted hexagons with different ground-state edge structures. In

growth or nucleation, energy variation enters exponentially as $\sim e^{\delta E/k_B T}$, strongly amplifying the symmetry breaking, up to completely changing the shapes to triangular, ribbonlike, or rhombic.

On some stages of growth, CNTs and graphene differ considerably, for example, during the nucleation. The honeycomb lattice tessellates the plane. After a stable planar nucleus is formed, graphene can grow by adding only new hexagons. While a CNT is a cylinder, which means that an initial carbon nucleus is topologically required to incorporate six pentagons exactly. A map of carbon nanoforms and their transformations using the number of hexagons N_6 and pentagons N_5 as coordinates is quite instructive (see Fig. 3a). Graphene islands/flakes of any size are represented by the $N_5 = 0$ line, with $N_6 \to \infty$ being the ideal infinite honeycomb lattice. One to five pentagons represents the small family of carbon nanocones whose angle at the tip has discrete values, depending on N_5.

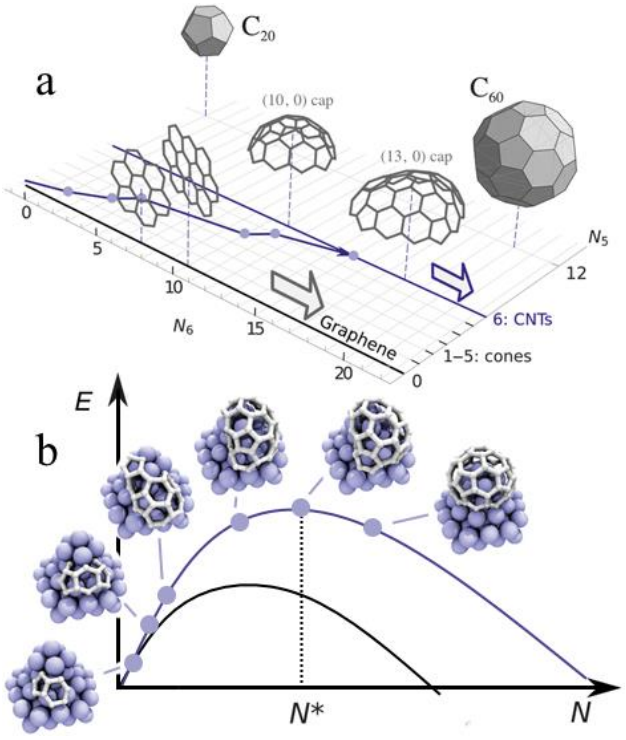

Figure 3. (a) Carbon forms projected onto the number of hexagons (N_6) and pentagons (N_5) coordinate plane. The blue line illustrates a gradual formation of a carbon nanotube (CNT) cap, with points indicating incorporation of a new pentagon. (b) Schematic energy profiles as a function of system size N for CNTs (blue curve; N* is the critical nucleus size) and graphene (black curve). [4]

Once the $N_5 = 6$ line is reached, the corresponding hemispherical cap is suitable to evolve into a cylinder, or liftoff the catalyst surface, unlike the graphene that always remains grounded. From the point of view of classical nucleation theory (Fig. 3b), the trajectory in the (N_6, N_5) plane, leading to the $N_5 = 6$ line, increases in energy to reach the critical nucleus cap of N* carbon atoms. In fact, the cylindrical topology of a CNT is a reason for the chirality of the nanotubes, and chiral indexes (n,m) describe the direction of the cylinder roll up through the chiral vector $C = n\,a_1 + m\,a_2$, where $a_{1,2}$ are the honeycomb lattice vectors.

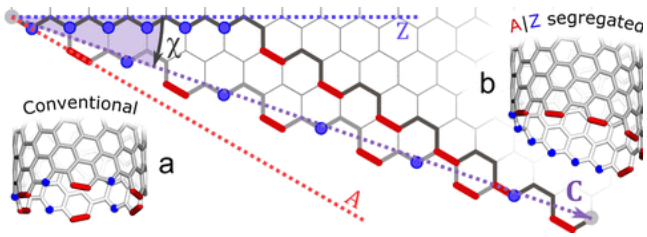

Figure 4. Two limit cases of edge configuration on the example of the (12,6) tube: (a) perfectly intermixed Z and A sites in the CE and (b) perfectly segregated sites in the A|Z-edge. [5]

As is clear from Fig. 3b, the energetics of the CNT in contact with the catalyst is essential for the determination of the nucleated nanotube. In practice, the interface energy of the carbon edge on the catalyst surface is used to estimate the probability of the nucleation for tubes of various chiralities as $p_{n,m} \propto \exp\left(-\frac{\Gamma_{n,m}}{k_B T}\right)$, where $\Gamma_{n,m}$ is the interface energy for (n, m) CNT, and T is a growth temperature. Unsurprisingly, the exact atomic structure of the interface affects its energetics playing a crucial role. Conventionally, only the simplest edge structure closely following the chiral vector was considered (Fig. 4a). If one would consider

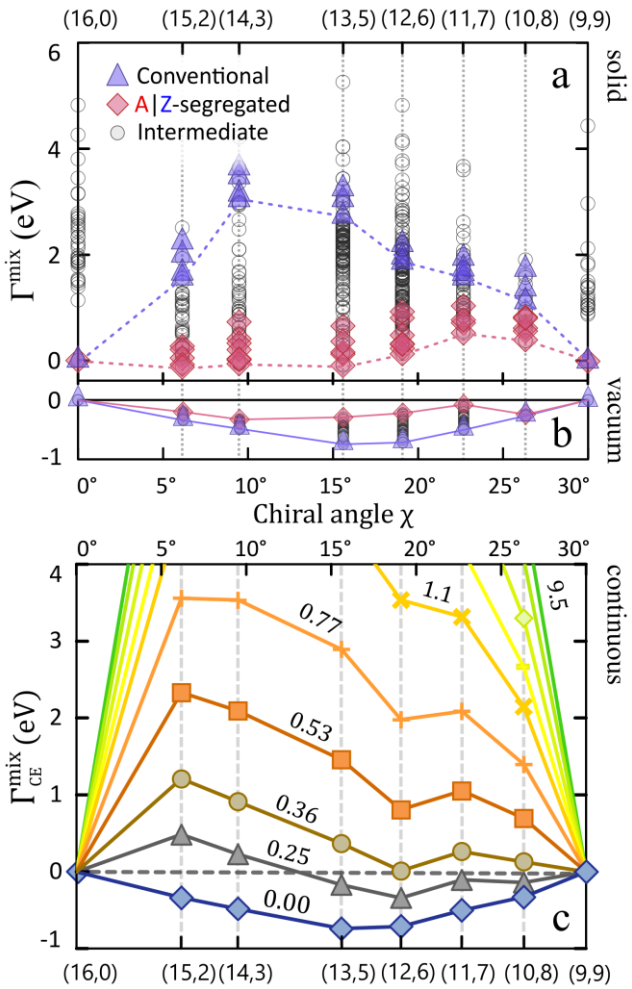

Figure 5. Edge mixing energy from ab initio calculation for a limited set on SWCN indicates strong preference towards edge segregation on solid Co_7W_6 substrate (a) and almost identical energies with small preference towards conventional edge in vacuum (b). Continuous substrate representation demonstrates transition from favoring conventional edge to strongly favoring segregated configuration with increased rigidity of the substrate (c), numbers indicate width parameter of the Morse potential α. [5]

CNT edge as a combination of *m* armchair (A) and *(n-m)* zigzag (Z) sites, then conventional edge (CE) of the nanotube represents a perfect mixture of those sites. However, this is not the only possible edge configuration, as A and Z sites can be partially or completely segregated within the length of the interface. Structure with fully separated sites – A|Z segregated edge – represents case polar opposite case to CE (Fig.4b). Interestingly, the number of A and Z sites and, hence, number and type of broken bond on the edge of the CNT is identical for both configurations. Then interface energy difference must be related with mixing of A and Z sites within the edge:

$$\Gamma_{n,m} = (n-m)\varepsilon_Z + m\varepsilon_A + \Gamma_{mix},$$

where ε_Z and ε_A are energies of Z and A sites respectively and Γ_{mix} is mixing energy. Furthermore, all intermediate edge configurations should lay between CE and A|Z configurations.

First, for simplicity we first considered a small set of nanotubes with extremely close diameters $d \approx 12.5$ Å: (16,0), (15,2), (14,3), (13,5), (12,6), (11,7), (10,2) and (9,9). Using first-principle calculations, we determined that in contact with solid W-terminated (003) Co_7W_6 catalyst surface A|Z-segregated configuration showed energies up to 4 eV lower than CE, being, in fact, the lowest energy configuration found through extensive translational and rotational search for variety of edge configurations (Fig.5a, note that for each edge configuration multiple relative positions on the substrate are possible). CE structures showed standard "hat-shaped" energy profile (purple line in Fig.5a) with chiral tubes showing energy significantly higher than achiral CNTs, corresponding to strong nucleation preference towards the latter; A|Z-segregated energy profile is almost flat with nucleation preference towards chiral (15,2) nanotube (Fig.4a pink line). Important to mention, that achiral and next-to-achiral tubes do not have corresponding A|Z segregated configuration.

Further consideration showed that in a vacuum this preference is reversed, with CE being slightly lower in energy. This observation inevitably leads to the conclusion that the state of the catalyst (vacuum can be thought of as a gaseous catalyst with $\varepsilon_Z = \varepsilon_A = 0$) can significantly influence favored edge structure (Fig.5b).

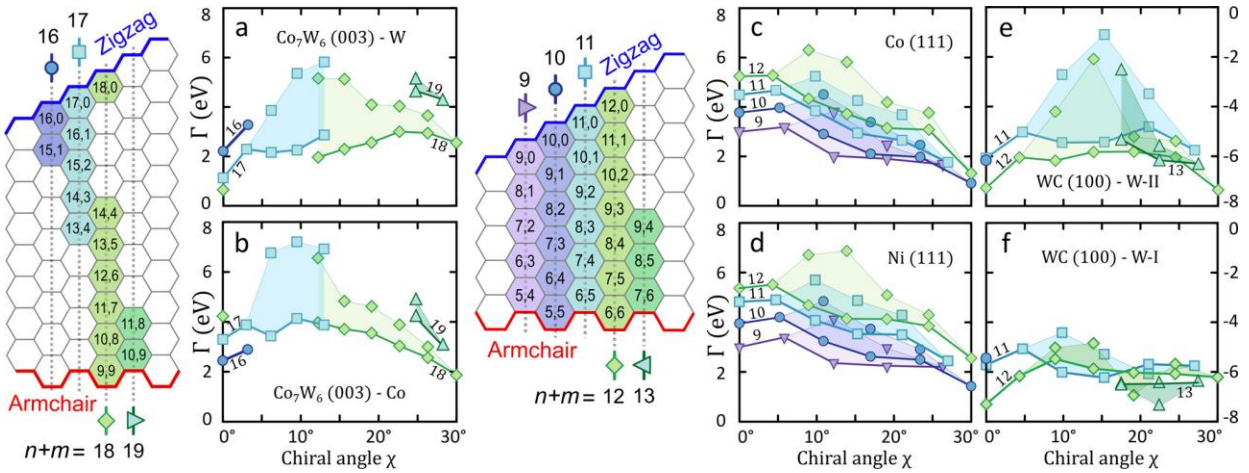

Figure 6. Interface energy Γ(χ) of CNTs on solid substrates: W- (a) and Co-terminated (b) Co_7W_6 (003) surfaces; closed-packed (111) surfaces of Co (c) and Ni (d); rigid (e) and "soft" (f) W-terminated WC(100) surfaces. Chiral maps show the computed (n, m) for the corresponding substrates. Solid lines indicate $\Gamma_{A|Z}$, and filled area shows energy difference between A|Z and CE. Symbols correspond to various numbers of edge atoms (n + m). [5]

Taking into account that CE has maximum and A|Z-segregated edge has the minimal number of A-Z interfaces, one can assume that the absolute value of mixing energy for a conventional edge would always be larger $\left|\Gamma_{CE}^{mix}\right| > |\Gamma_{A|Z}^{mix}|$. Then, analogs to vicinal surface segregation in 3D, CNT edge segregation preference can be concluded just from the sign of the Γ_{CE}^{mix}. To simplify the model, we excluded atomistic resolution within the substrate and represented it as a continuous Morse surface:

$$V(r) = V_0\left(1 - e^{-\alpha(r-r0)}\right)^2,$$

where V_0 represents the strength of the interaction between the edge of the CNT and catalyst while width parameter α characterizes the compliance of the substrate surface. Using continuous substrate model we determined that infinitely compliant catalyst, similarly to vacuum, favors CE configuration, medium values of compliance (liquid catalyst) result in mixed preference or favor A|Z configuration, and high rigidity of catalyst results in strong preference towards edge segregation (see Fig.5 c).

Using first-principle calculations, we determined interface energies of a wide range of CNTs on several representative substrates: W- and Co-terminated (003) surfaces of Co_7W_6 catalyst, (111) surfaces of Co and Ni, and two types of W-terminated WC (100) surface. Universally, A|Z-segregation resulted in a significant decrease in the interface energy of chiral nanotubes (see Fig.6). In fact, for Co_7W_6 (003) and WC (100) surfaces due to close values of interface energies between the armchair and zigzag nanotubes interface energy profile for A|Z edge is almost horizontal with probability of nucleation of chiral CNTs on par or exciding that for the achiral tubes. This observation is consistent with both of those solid catalysts being used to experimentally produce CNT populations with high preference towards chiral (12,6), (14,4) and (8,4) nanotubes. For monometallic Co and Ni catalyst CNTs edge segregated configurations are also preferred, but strong energetic preference towards armchair nanotubes compared to the zigzag nanotubes results in energy profile skewed towards higher chiral angles; consistently experimental growth on such catalysts results in preference towards next-to-armchair CNT as we show below. This uncovered universal trend for edge segregation not only provides theoretical explanation to recently observed experimental results but also offers a richer basis for general understanding, modeling, and control of catalytic CNT synthesis.

Experiments in catalytic growth over the last decade have repeatedly revealed a strong puzzling preference towards minimally chiral (near-armchair) tubes (see (6,5) and (9,8) peaks in Fig.1) on Co and Ni catalytic

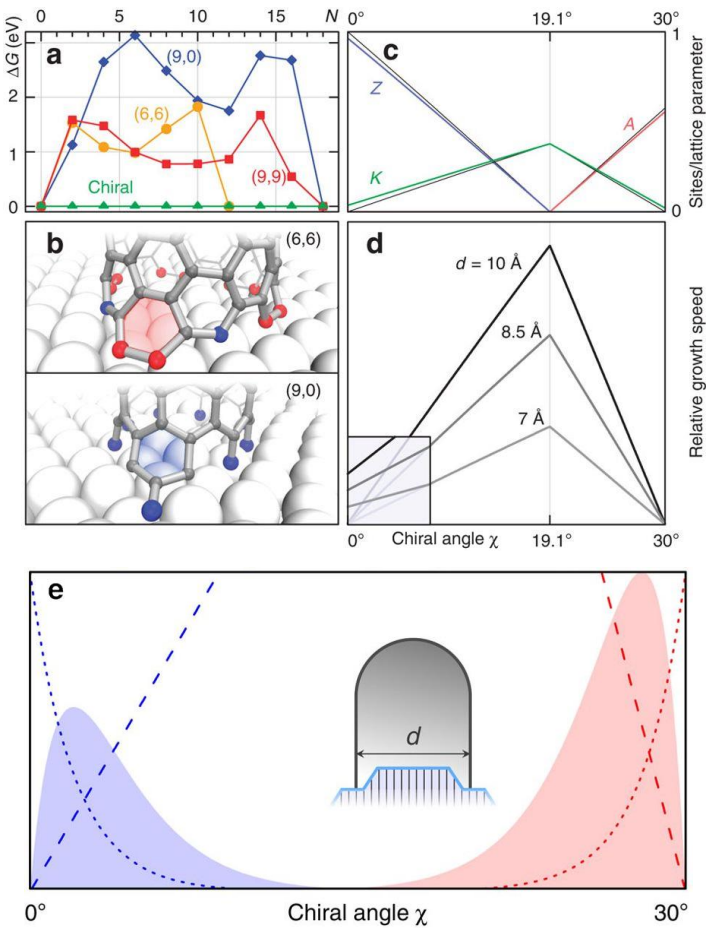

Figure 7. (a) Free-energy profiles during the growth of a new ring of hexagons on (red, orange) A and (blue) Z edges as a function of number of added atoms N. The green line corresponds to barrierless chiral-edge growth. (b) The atomic configurations after first dimer addition, N=2. (c) Linear density of different site types on CNT edges as a function of chiral angle. (d) The resulting CNT growth rate as a function of chiral angle for several diameters (inset shows the effect of thermal kinks). (e) The abundance distributions $A(\chi) \sim \chi\, e^{-\chi}$ computed as the product of nucleation $N_{n,m}$ (dotted) and growth rate $R_{n,m}$ (dashed) terms shows a near-Z (blue) and near-A (red) chiralities depending on tilt of energy preference. [6]

particles, challenging any existing hypotheses and making chirality control ever more tantalizing, yet leaving its understanding elusive. We propose to treat the CNT abundance by type as the result of the action of two main factors. At proper conditions, the nanotubes nucleation occurs, with probability $N_{n,m}$ for certain chiral type (n,m). It is followed by the steady carbon accretion by each tube, with its growth rate $R_{n,m}$. After some time, the fraction of the tubes of chirality (n,m), that is, their relative abundance $A_{n,m}$ in the accumulated material, is determined by the product of both these factors, as:

$$A_{n,m} = N_{n,m} \times R_{n,m}.$$

As we showed earlier on Co and Ni surfaces thermodynamically driven nucleation would result in strong preference towards achiral armchair nanotubes (Fig.6 c,d). However, such low energy indicates an extremely stable interface between the CNT edge and metal due to a simple flat-to-flat configuration. Aside from the high nucleation rate it would also indicate that addition of new carbon to the nanotube edge in this configuration would be extremely hard due to absence of appropriate adsorption sites. The energetic profiles characterizing the sequential carbon addition (Fig.7), obtained through the first principle calculations, show extremely high barriers for achiral nanotubes. The CNT growth rate $R_{n,m}$ can be related to the number of the adsorption sites on the edge of the CNT, resulting in kinetic preference towards chiral nanotubes (Fig.7d).

Continuous consideration for tubes of very similar diameters (which is commonly controlled by the size of the catalytic particles) yields relation between the chiral angle and nucleation probability $N_\chi \propto e^{-\beta x}$, where x is the angular deviation from the achiral direction and $\beta = \frac{\pi d \gamma'}{k_B T}$ (note that this expression accurately represents only neighborhoods of the achiral tubes while nucleation away from this region is extremely unlikely). Growth rate can also be expressed as $R \propto x$. In this case for the armchair side where $x = \chi^-$ CNT abundance:

$$A(\chi) \propto \chi e^{-\chi}.$$

Therefore, the combination of the nanotube/catalyst interface thermodynamics with the kinetic growth theory is able to explain preference towards the nanotubes with one-off chirality (Fig. 7e). The unusual abundance peaks emerge from the two antagonistic trends at the interface: energetic preference towards achiral versus the faster growth kinetics of chiral nanotubes. Combining this with investigation of the catalyst-CNT edge interaction we showed earlier leads to conclusion that such behavior would be observed only in cases where interaction with the substrate strongly favors either zigzag or armchair side of the chiral angle spectrum. For the Co (111) surface specifically, the thermodynamic preference towards the armchair CNTs leads to the increasingly high abundance of the next-to-armchair (6,5) nanotubes.

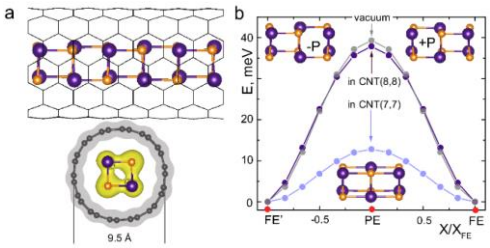

Figure 8. (a) Top: sketch of SnS nanowire in SWCNT; bottom: computed charge density isosurface. (b) Energy change as a function of atom displacement *X*, in vacuum, inside (8,8) and (7,7) CNT. [8]

Finally, our investigation into a novel use of the CNTs – as the encapsulation of the 1D ferroelectric GeS and SnS nanowires – revealed the domain wall localization, switchable carrier mobility, and practically effective shieling. The effect of CNT is demonstrated on the example of the SnS. Simulating the experimental situation, an SnS nanowire is placed in the center of CNT of various diameters, Fig. 6a. The formation (adsorption) energies for the SnS@CNT calculated to be -0.71 eV/f.u. and -1.99 eV/f.u. for (8,8) and (7,7) CNT, respectively. The repolarization energy barrier E_p is also decreased in smaller-diameter CNT, Fig. 6b, leading correspondingly to lower Curie temperature.

Publications from this reporting period

[1] R. Rao, C.L. Pint, A.E. Islam, R.S. Weatherup, S. Hofmann, E.R. Meshot, F. Wu et al. "Carbon nanotubes and related nanomaterials: critical advances and challenges for synthesis toward mainstream commercial applications." *ACS Nano* 2018, **12**(12), pp. 11756-11784. DOI:10.1021/acsnano.8b06511.

[2] Q. Yuan, B.I. Yakobson, and F. Ding. "Edge-Catalyst Wetting and Orientation Control of Graphene Growth by Chemical Vapor Deposition Growth." *J. Phys. Chem. Lett.*, 2014, **5** (18), pp 3093–3099. DOI: 10.1021/jz5015899.

[3] V.I. Artyukhov, Y. Hao, R.S. Ruoff, and B.I. Yakobson." Breaking of Symmetry in Graphene Growth on Metal Substrates". *Phys. Rev. Lett.*, 2015, **114**, p.115502. DOI: 10.1103/PhysRevLett.114.115502.

[4] E.S. Penev, F. Ding, and B.I. Yakobson. "Mechanisms and theoretical simulations of the catalytic growth of nanocarbons." *MRS Bulletin* 2017, **42**(11), pp. 794-801. DOI:10.1557/mrs.2017.236.

[5] K.V. Bets, E.S. Penev, and B.I. Yakobson. "Janus Segregation at the Carbon Nanotube-Catalyst Interface." *ACS Nano* 2019, **13**(8), pp. 8836-8841. DOI:10.1021/acsnano.9b02061.

[6] V.I. Artyukhov, Y. Hao, R.S. Ruoff, and B.I. Yakobson." Breaking of Symmetry in Graphene Growth on Metal Substrates". *Phys. Rev. Lett.*, 2015, **114**, p.115502. DOI: 10.1103/PhysRevLett.114.115502.

[7] R. Ye, Y. Liu, Z. Peng, T. Wang, A.S. Jalilov, B.I. Yakobson, S.-H. Wei, and J. M. Tour. "High Performance Electrocatalytic Reaction of Hydrogen and Oxygen on Ruthenium Nanoclusters." *ACS Appl. Mater. Interfaces*, 2017, **9** (4), pp 3785–3791. DOI: 10.1021/acsami.6b15725.

[8] J.-J. Zhang, J. Guan, S. Dong, and B.I. Yakobson. "Room-temperature ferroelectricity in group-IV metal chalcogenide nanowires." *J. Am. Chem. Soc.* 2019. DOI:10.1021/jacs.9b03201.